0609

APPLICATION OF X-RAY COMPUTED TOMOGRAPHY FOR ANALYZING CLEAT ANGLE, SPACING AND APERTURE DISTRIBUTION IN LARGE COAL BLOCKS AND CORES

Saikat Mazumder, Karl Heinz Wolf, Koenraad Elewaut and Rudy Ephraim
Department of Geotechnology, Delft University of Technology, The Netherlands

ABSTRACT

New techniques to determine distributions of cleat aperture, cleat orientation and cleat spacing from CT scans have been developed. For cleat orientation and spacing distributions, two different coal blocks were scanned. The CT scans have been analysed for the three orthogonal directions. Histograms of the cleat orientations are bimodal, expressing the typical cleat texture of face and butt cleats and bedding perpendicular relaxation fractures. Deviations up to 20° from the peak values in the cleat orientation distributions were used as input for automated image analysis of cleat spacing. Distributions of the cleat spacing measurements are related to the face and butt cleat directions. The term "relevant cleat length" is introduced as a measure to extract the amount of cleat length involved with the cleat spacing measurements. The ratio ranges from 0.03 to 0.38 and expresses the difference in cleat texture in both samples. Cleat spacing versus relevant cleat length shows sample specific patterns for face cleat, butt cleat and bedding.To describe cleat aperture quantitatively, peak height and missing attenuation have been used. The image of a cleat was seen as a convolution of a rectangular fracture profile with a Gaussian point spread function.

INTRODUCTION

The cleat network of coal plays an important role in the production of methane from coalbeds. While micropores are responsible for most of the porosity in coal, the cleats provide the principal source of permeability for fluid flow. Coal beds have two major orthogonal joint systems called face cleats and butt cleats. Key cleat attributes include size, spacing, connectedness, aperture, degree of mineral fill, and patterns of preferred orientation on local and regional scales [3]. These cleat attributes are important for flow parameters and are needed as input in coal reservoir models. The dominant flow direction is related to the existing cleat system and is controlled by the Darcy permeability. Very few data are available on the aperture, height, length, and connectivity of cleats. Bertheux [2], and Wolf et al. [17], used a comprehensive way to determine cleat angle in coal seams using image analysis techniques. With coal particles, cleat angle distribution was analyzed for face cleats, butt cleats and bedding. In addition an attempt was made to determine cleat spacing distribution, based on differences in fracture behaviour of the macerals and ash. However, applied to cuttings, which are affected by transport, only angle distribution can be reconstructed.

Cleat spacing is on the order of a millimeter to centimeter, so numerous fractures are typically present in coal cores. However, core observations rarely distinguish the hierarchy of fracture sizes that are present. Recognizing the wide range of cleat sizes present in coal, quantitative density analysis is only meaningful when cleat size is included in an analysis.

Variability in spacing (or intensity of fracture development) of cleats in coal beds has already been recognized by Kendall and Briggs [7]. Contrasts in coalbed methane production also may reflect variable development of cleats. Researchers have observed that cleat spacing varies with coal rank, decreasing

from lignite through medium volatile bituminous coal [1, 12, 9] and increasing through the anthracite range, forming a bell shaped distribution of cleat spacing. Based on outcrop and core data from North American coal, Law [9] found that face cleat spacing ranges from approximately 22 cm in lignites (% R_r 0.25 - 0.38%) to 0.2 cm in anthracites (% R_r more than 2.6%). Many authors have noted that cleat spacing varies with coal type and ash content [13, 9]. Bright coal lithotypes (vitrain) generally have smaller cleat spacings than dull coal lithotypes (durain) [7, 10]. Coals with low ash content tend to have smaller cleat spacings than those with high ash contents [8]. It has been found that average cleat spacing is linearly proportional to coal lithotype layer thickness [13, 3, 9]. Our study tries to overcome the limitation of hierarchy of fracture sizes and proposes a technique to measure and compare cleat spacing distributions from Computer Tomography (CT) scan images of coal blocks. Since the accuracy of cleat determination from CT-images depends on the pixel size, images have to be enhanced to obtain the smallest cleats possible. Fractures are recognized by either change in the CT-number (attenuation coefficient) and/or low number grey values, which can be followed in a certain direction.

Cleat aperture width under in situ conditions is an important attribute of cleat geometry and permeability. The collection of aperture data under stressed conditions is difficult to determine because of the low resolution. However cleat aperture data under non stressed conditions are available and is of importance for spatial analysis. For example, face cleat aperture measurements of six relaxed Fruitland coal cores from the northern San Juan basin vary in range from 0.01 mm to 0.30 mm [3]. Cleat aperture widths under in-situ confining pressure probably vary from less than 0.05 mm to less than 0.0001 mm. Karacan et al. [5] did a similar study to understand the cleat aperture distributions for some Turkish coal samples. We used a non-destructive core scanning technique to obtain cleat aperture distribution from a Polish and an English coal sample under unstressed conditions.

Hence, in this paper new methods are introduced to determine cleat aperture, cleat orientation and cleat spacing distribution with CT-scans.

SAMPLE DETAILS

The samples used for cleat spacing measurements were from a French coal mine (France 495) and from the Upper Silezia mine in Poland (Brzeszcze LW 405). Both samples were lumps of coal and were scanned as obtained. The Brzeszcze LW 405 was one of the target seams for CO_2 injection, as part of the project "RECOPOL". It has a vitrinite reflectance of 0.74%. The Brzeszcze mine is situated in the southeastern part of the Upper Silesian Coal Basin. This coal seam is Carbonigerous in age.

Of the two coal core samples used for cleat aperture measurement one was from the Silezia mine in the Upper Silesian Basin in Poland (Silesia 315). The coal was obtained as a hard sample from a depth of 900 m. This coal seam was also selected for CO_2 injection in the RECOPOL project. It is a high volatile bituminous coal from Pennsylvanian with a vitrinite reflectance of 0.68%. A cylindrical core of 7 cm in diameter and 25 cm in length was drilled out of the block. The other coal core (Tupton) used for this purpose has similar dimensions and was obtained from the Nottinghamshire and North Derbyshire coal mines in UK. The Tupton sample is of Westphalian A age and had a vitrinite reflectance of 0.53%. The sample details are gathered in Table 1.

DATA ACQUISITION AND PROCESSING PROCEDURE

The X-ray CT scanner measures the X-ray absorption through the linear attenuation coefficient, μ, which is defined as:

$$\mu = \left(\frac{1}{L}\right)\ln\left(\frac{I}{I_0}\right) \tag{1}$$

The CT scanner readings are usually reported in the form of a so-called CT number, or Houndsfield unit, which is defined as:

$$CT_N = K\left(\frac{\mu - \mu_w}{\mu_w}\right) \tag{2}$$

For cleat spacing and orientation measurements, CT scan images were produced by the Institute Francais du Petrol in Paris. Using a General Electric, SX/I high-speed sequential CT scanner the images were made as sequential scans in RAW and JPEG format at a resolution of 512 x 512 pixels with 256 grey levels. Each pixel in the XY plane represents an area of 0.7 x 0.7 mm. The distance between two images in the scan direction was 1 mm. The images were enhanced in order to increase the contrast between matrix, fracture and mineral filled fracture. This also gave way to a better discrimination of increased artifacts, like scattered noise and a diagonal linear pattern [6].

A set of images from a CT scan session is usually called an image stack. The section plane is the XY plane and the scan direction is the Z axis. For viewing and for extracting 3D information from the image stacks the 3D visualisation and modelling software Amira™ was used. Image stacks in the orthogonal YZ and XZ directions were generated, saved as JPG images, providing a complete set of images in all three orthogonal directions (Fig. 1). QWIN™, image analysis software was used to correct for the beam hardening effects, which were induced by high density spots in the sample. In each image the cleat spacing, coal matrix and mineral matter were seperated by grey tones. Then each image was processed in order to supress details that were not contributing to the required information, i.e. lines and spots. Thereafter the resulting binary images for cleats, mineral matter and matrix were used for measurements. Ample care was taken to remove only noise and artifacts.

The mentioned artifacts introduced two difficulties:

(i) Incomplete cleat detection, and

(ii) Scattered vesicles, detected as cleats but with a high ambiguity.

The described image complexities made it necessary to improve each image both manually and automatically. The automatic procedure consists of a sequence of image analysis processes called erosion and dilation, using for these elongate cleat elements, linear operators (or kernels, or structuring elements) in eight different directions. It resulted into a suppression of all non linear binary objects, leaving the continuous cleat lines unaffected. The manual procedure followed, was completing detected cleat structures that, otherwise visible in the original image, were 'broken' due to the above mentioned resolution features. All remaining artifacts were erased. Thereafter cleat lines were thinned by an erosion procedure called skeletonisation, leaving lines 1 pixel wide through the middle of the cleats. Next, where two cleats crossed or a cleat suddenly changed direction, the lines were split, making orientation measurements possible on the resulting segmented lines. These sequences of enhancements provided images, which were saved for further analysis.

The orientation and lengths of all cleat line segments in a stack of images were measured, after first calculating a best fit. The goal of these measurements was to find the two main cleat directions: face and butt cleats. This was necessary for measuring the cleat spacings of sub-parallel cleats. A histogram of the frequency distribution showed the expected bimodal behavior. Next, a QWIN™ program was developed to find the cleat spacings for all cleats in a particular direction, i.e. face, butt or bedding, using the steps (Fig. 2):

(i) Input of the orientation of the cleats for which the spacings were measured.

(ii) Suppressing cleats outside the direction of the pre-defined orientation and a spread around this value.

(iii) Adding a grid of parallel lines to the image with the orientation perpendicular to the pre-defined cleat direction and with a spacing of 4 pixels corresponding to the smallest cleat length measured.

(iv) Only accepting lines or line segments that had connection from one cleat to another.

(v) Measuring all accepted line segments giving the desired cleat spacings.and producing their frequency distributions.

In order to relate the measured and distributed cleat spacings to the cleat lengths involved, the originally measured number of spacing line segment per class (bin) is recalculated to the summed cleat length used for cleat spacing, using the following equation:

$$U = ((F - 1) * G) + 1 + n \qquad (3)$$

As *U* is based on counting the number of line segments with a space of 3 pixels between the grid lines, resulting in an accuracy of +/- 6 pixels, the constant *n* (here is 3) expresses the integer of the average accuracy range in pixels.

Adding *U* for all distribution frequencies gives a value for the total cleat length involved with the spacing measurement. This result can be found in Table 2, column sum cleat lengths for spacings (px) and expresses an estimation of the total length of cleats:

- within the preferred orientation range
- with a minimum length of 4 pixels
- with at least one other cleat opposite on order to measure their distance.

It is possible that a cleat is parallel with two other cleats at both sides and with the same distance. In this case the cleat length related to the spacing is included only once. As this situation has a probability related to the cleat density, the discussed cleat length values are estimation.

Cleat aperture measurement from CT scans

The X-ray CT scanner used in this study is SOMATOM Volume Zoom quad-slice, manufactured by Siemens. In this third generation apparatus, the X-ray source-detector system rotates continuously for whole object examinations using traversing slice method. The imaging system uses the Somaris software to reconstruct the images of the subject, from multidirectional transmission data. The scanner operated at 120 KV and 165 mA. The scanning time was 2 seconds per slice (multi-scan technique). The reconstruction matrix consisted of 512 by 512 pixels. The X-ray source has a 0.8 x 0.9 mm spot size and the detector is made of 768 multi-used chambers. The apparatus allows a minimum slice thickness of 0.5 mm. Slice thickness of 0.5 and 1 mm have been used for this study. Each pixel in the XY plane represents an area of 0.29 x 0.29 mm.

Cleat apertures are discernible as a reduction in the CT number for the pixel containing the cleat, relative to pixels which are 100% coal matrix. Since the images are usually seen as monochromatic, with the lowest CT number set to black and the highest to white, the reduction in CT number is seen as a darker grey, as shown in Fig. 3a. This image presents a typical scan of a cleated coal. Air seen as black, with CT_{air} = -1000. As can be seen from Fig. 3b a dip in the profile is noticed where the cleat is present. In theory, the image of a cleat can be seen as a convolution of a rectangular fracture profile with a point spread function (PSF), which is Gaussian (Fig. 4), Vandersteen et al., (2003). The variability in the matrix CT numbers is due to differences in maceral composition for the coal. The CT scanner is calibrated with a water phantom and using Eq. (2), this yields values of 0 for water and -1000 for air. Although it is possible also to calibrate the CT scanner using other materials (e.g. carbon, as a material close in density to coal) this does not acually affect the data, but rather the scale on which the data is presented. Rescaling by using a coal analogue phantom, changes the amplitude of the dataset enhancing the signal of features such as cleats. At the same time this rescaling affects the expressed values of noise artefacts that in the end are more dominant in the resolving limit for cleat aperture measurement. So, although the features in the coal stand out at higher amplitude and are thus in theory more easy to distinguish, the values caused by noise artefacts are also increased with the same amplitude.

Several parameters have been described to quantitatively describe the cleat apertures as shown in Fig. 3c. These parameters are listed and compared by Vandersteen et al., 2003. A missing rock mass or a missing attenuation (*MA*) is described as the integrated loss of the attenuation coefficient due to the presence of the cleat. Alternatively peak height value (*PH*) of the attenuation profile was used to measure the aperture (Verhelst et al., 1995). The advantage of peak height (*PH*) is that it's independent of the direction of measurement in the cleat. Missing attenuation on the other hand needs to be measured perpendicular to the direction of the fracture plane (Van Geet, 2001). In the present study we used both the parameters to describe cleat aperture with a proper calibration technique. Generally, images which have a very high signal to noise ratio, the missing attenuation (*MA*) and peak height (*PH*) can be directly estimated. However the heterogeneities in coal render the images with a very low signal to noise ratio. Thus an alternative fitting procedure is used to calculate *MA* and *PH* of a cleat in coal.

The dip in the attenuation profile is fitted by a Gaussian point spread function. The background noise due to the presence of heterogeneities can be averaged out to derive the near CT host rock response. The averaging was done using a certain tolerance in the measurements. Thus an attenuation profile 'Y' containing a cleat can be described as,

$$Y = PH \exp\left[-\frac{1}{2}\left(\frac{X - xp}{\Delta xp} \right)^2 \right] + CT_{coal} \tag{4}$$

Missing attenuation (MA) can be described as,

$$MA = \sqrt{2\pi . PH . \Delta xp} \tag{5}$$

Eq.s (4) and (5) are referenced in Vandersteen et al. [14]. As shown in Fig. 4b, this fitting technique approximates the measured data quite well. Fig. 4a represents the original data with the solid line as the mean CT of the coal matrix and the dotted line as the tolerance to calculate the average. Thereafter we assume a Gaussian function of the form

$$f(x) = A \exp(-Bx^2) \tag{6}$$

Following the procedure to minimize the least square error leads to a set of non-linear equations for the coefficients A and B. To generate a solution, the least-square error was minimized. In particular, the sum

$$E_2 = \sum_{k=0}^{n} \left| A \exp(-Bx_k^2) - y_k \right|^2 \tag{7}$$

was minimized using the MATLAB routine. An initial guess of the parameters were required to do the minimization. This method does the non-linear Gaussian fit to the data from each attenuation profile (Fig. 4b) and returns the optimized values of PH, MA and xp.

With the whole set of optimized values of PH and MA from each of the scanned coal cores, a proper calibration was needed to translate the data to meaningful aperture measurements. Cleat aperture calibration standards were constructed for this purpose. The calibration standard comprised two halves of the same coal type. The adjoining flat surfaces were polished, to reduce surface roughness. To produce a "fracture" of known aperture, two metal feeler gauges of calibrated thickness were placed between the two flat surfaces. The two halves were firmly held together with a clamp during scanning and the lower polished surface was leveled, to produce a horizontal fracture plane. The scan was done perpendicular to the longitudinal axis of the calibration standard, between the two feeler gauges. Fracture apertures ranging from 0.05 mm to 0.63 mm were scanned.

RESULTS AND DISCUSSION

Cleat orientation and spacing measuments

For two samples, France 495 and Brzeszce LW405, the cleat spacing distribution was measured in the three orthogonal directions. The France 495 sample was scanned in one direction. The Polish sample was scanned in two orthogonal directions because of the image quality. Of the French sample the calibration values are known (0.7 mm per pixel in the XY plane, 1 mm per pixel in the YZ and ZX planes), but from the Polish sample there is no calibration information. Hence, all results are discussed in pixel units. Moreover, to describe a method to measure cleat spacing distribution, it is not needed to give results in absolute values other than pixels.

To recognize the statistical value of the outcomes, the results are split up in:

(i) Total lengths of open cleats and cleat orientation distribution. All cleats are measured in all directions within a stack. Cleat orientation distribution is related to the section plane in which an image stack is oriented. In all images the zero orientation points horizontal, the angles turning clockwise.

(ii) Lengths of cleats in the preferred orientations. From the orientation distribution (Figs. 5 and 6) the preferred angles are selected with a certain spread. The cleats within the defined angle range are used for cleat length measurements.

(iii) Total cleat lengths used for cleat spacing measurement. Those oriented sub-parallel cleat segments that can be used for cleat spacing measurements are selected on summarized cleat length and spacing distribution. Total cleat lengths used for cleat spacing measurement divided by the total lengths of open cleats gives the relevant cleat length ratio.

Cleat orientation distributions

Table 2 shows for both samples the major cleat orientations, divided in face and butt cleats in the XY and ZX directions respectively, and relaxation fractures (sub-) parallel to the bedding, for the ZY planes. For comparison all results are presented in pixels. The table shows that genuine cleat systems can be recognized by high relevant cleat length ratios. In other words, a face cleat and a butt cleat system are clearly recognized, when measured and ordered according to the preferred cleat orientations. For example, for France 495 the XY plane 0° and the ZY plane 90° have a relevant cleat length of 0.26 and 0.54 respectively. When looking at Fig. 7a and f, the related summed cleat spacing distributions are high with maximum values of respectively 12000 and 5500 pixels. It can be concluded that the face cleat system, which is oriented sub-parallel to the ZX plane, has a regular spacing distribution. Considering the butt cleat system, which usually is more random and here oriented sub-parallel to the XY plane, the relevant cleat length has a lower ratio for the ZX plane 0° and ZY plane 0° of respectively 0.11 and 0.04. For the bedding, oriented according to the ZY plane, intermediate ratios are measured of 0.14 in the XY plane 90° and 0.21 in the ZX plane 94°. Also for the orientations of the butt cleats (Fig. 7c and e) and bedding planes (Fig. 7b and d) the cleat spacing distributions in different directions show similar shapes. From the shapes it can be concluded that the cleat spacing distribution, measured over the same volume in perpendicular distances, give comparable results. However, pixel counts can be different, since the XY plane and Z direction have different resolutions attributed to the pixel size. The spreading and summed pixel counts for the spacing in the three directions are a measure for the regularity of the cleat texture. Higher counts mean more relevant cleat length in a specific direction (Fig. 7a and f). Wide peak distributions count for a large spread in cleat spacing (Fig. 7b and d). An irregular spacing pattern represents dispersed cleat spacing in one specific direction (Fig. 7c and e). For the France 495 series, the most pronounced cleat spacing distribution is found for the face cleats. Fig. 8 shows a rendered pseudo 3D representation in Amira of the detected cleats structure in the France 495 sample and Fig. 9 a schematic drawing of the found cleat and bedding directions.

Cleat spacing distribution

Fig. 10 shows the spacing distributions parallel to the cleats and bedding for the Brzeszce LW405 sample. The spacing distribution in all directions is poorly pronounced when compared to the France sample. Both Table 2, Figs. 5 and 6 shows that the values for cleat length, relevant cleat length and cleat orientation distribution for Brzeszce samples are low, which point to more random cleat dispersion. This is clearly visible in the spacing distributions of the bedding plane cleats (Fig. 10b and d), face cleats (Fig. 10a and f) and butt cleats (Fig. 10c and e). The moderate quality of the CT scan images meant that, only the face cleats in the XY-plane and butt cleats in the XZ-plane could be used.

The reasons of the poor cleat distribution properties of the Polish sample are:

- Less cleats are present in the coal block, so less total cleat length is available (Table 2).

- Less cleats are measured (one order of magnitude less) in cleat orientation measurements for Brzeszce compared to the French sample.

Since the samples are from different regions, they have different burial history and consequently a difference in cleat orientation and in cleat spacing behavior.

The cleat orientations of the France 495 and the Brzeszce LW405 sample (Figs. 5 and 6) show comparable major cleat orientations. So, the cleat planes in both samples run sub-parallel to the XYZ planes. However, the difference between the samples can be found in the spread which is much higher for the France 495. Based on frequency distributions this sample also shows a higher cleat density. When considered the angle orientations between 30° and 80° and between 110° and 160°, the Brzeszce 405 sample shows a more pronounced cleat system.

The cleat spacing distributions of the France 495 sample are, as with cleat orientation, more detailed compared to the results of the Brzeszce sample. We observed that the spread in cleat orientations also results in a larger spread of cleat spacings. The results of cleat spacing distributions are all negatively skewed. It is not known whether it is common to have cleat spacing distributions log-normally distributed or the skewness is because of some other reasons.

Cleat aperture measurements

Using the calibration method described above, fracture apertures ranging from 0.05 mm to 0.63 mm were scanned for coal to obtain a calibration curve. The calibration curves for peak height (PH) and missing attenuation (MA) are shown in Fig. 11a. The figure also shows that missing attenuation (MA) as a function of the cleat aperture, yields a more curvilinear relationship as compared to the peak height (PH). The slope of MA initially has a higher value and decreased with increasing cleat apertures. Thus the missing attenuation is a more sensitive parameter than peak height (PH). This is quite understandable as the missing attenuation is more sensitive to the direction in which the profiling is done. Also the fact that MA is a derived parameter and is a function of PH and Δxp, it carries over the error from multiple parameters and generates more error. For near vertical cleats, the calibration profile for MA should be orthogonal to the cleat trace, whereas peak height is insensitive to the profiling direction. For non-vertical cleats, MA has to be multiplied with the co-sine value of the inclination of the cleat plane. 80 to 90 cleat attenuation profiles were analyzed for each cleat aperture calibration point. Fig. 11b is a plot of the coefficient of variation for both peak height and missing attenuation as a function of the aperture width. Missing attenuation (MA) is a better parameter while determining fractures of larger aperture widths. For lower aperture widths as can be seen from Fig. 11a, MA is highly sensitive and thus peak height (PH) is a better parameter to calculate cleat apertures. Thus for samaller apertures, where the measurement error for MA is large, the data should be used with scepticism.

Thus using peak height and missing attenuation as parameters to calculate cleat aperture widths, all measurements for the Silesia and the Tupton coals were used to derive the cleat aperture frequency distributions. Figs. 12a and 13a are the aperture distributions of the Silesia and the Tupton coal, using PH as a parameter. Figs. 12b and 13b are the aperture distributions of the Silesia and the Tupton coal, using MA as a parameter to calculate cleat apertures. For the Silesia coal (Fig. 12a and b), using peak height and missing attenuation as parameters to calculate cleat aperture, quite a variability of the aperture distribution is observed. While the mean aperture using PH was calculated to be 0.087 mm, using MA as a parameter it is 0.052 mm. As already discussed, MA is highly sensitive at lower cleat aperture widths. Thus for the Silesian coal, the aperture distribution calculated using PH as a parameter is more reliable. Whereas for the Tupton coal, the aperture measurements using PH and MA are both in good agreement with each other. The mean cleat aperture using PH as a parameter is 0.225 mm and using MA as a parameter is 0.247 mm.

ERROR ANALYSIS

The uncertainity principle was used to estimate the experimental error in measuring the missing attenuation and the peak height. The principle is based on the concept of calculating the uncertainity in the final value of the calculated parameter from the uncertainities of each measured variables [4, 11]. The effects of each measured variables on the final calculated variable value is derived from the concept of propagation of errors. The concept is best explained by the following example:

For evaluation of the uncertainity in the value of parameter R, where R is a function of independent variables (x_i), i.e.:

$$\mathbf{R} = \mathbf{R}(\mathbf{x}_1, \mathbf{x}_2, \mathbf{x}_3, \ldots\ldots\ldots\ldots\mathbf{x}_n) \tag{8}$$

where if U_R denotes the uncertainity in the result R and, U_i is the uncertainity in each variable x_i, then the uncertainity U_R is given by

$$\mathbf{U}_R = \left[\left(\frac{\partial R}{\partial x_1} U_1 \right)^2 + \left(\frac{\partial R}{\partial x_2} U_2 \right)^2 + ... + \left(\frac{\partial R}{\partial x_n} U_n \right)^2 \right]^{\frac{1}{2}} \quad (9)$$

Applying this concept for our case and starting with the equation for missing attenuation (Eq. 5), the measured independent variables are: PH and Δxp. Thus taking the partial derivative of MA with respect to the above mentioned independent variables, the uncertainity in missing attenuation is then derived as

$$\partial \mathbf{MA} = \sqrt{\left(\pi \frac{\Delta xp}{\sqrt{2\pi.PH.\Delta xp}} \partial PH \right)^2 + \left(\pi \frac{PH}{\sqrt{2\pi.PH.\Delta xp}} \partial \Delta xp \right)^2} \quad (10)$$

The independent variable PH (peak height) depends directly on how good is the averaging technique. An estimate of the standard deviations of all the "near host rock CT number" for the Silesia sample has been made, the results of which are shown in Fig.14. The average measured standard deviation for all 196 measured profiles is 28.4 (∂PH). The least error minimization leads to optimized values for PH, MA and xp. A pesimistic estimate of $\partial \Delta xp$ was around 0.2. Using Eq. 10 the values of ∂MA is calculated and has been plotted in Fig. 15. The average calculated error for the missing attenuation (MA) was 15.8%. A realistic estimate of $\partial \Delta xp$ would be around 0.1 and that would yield an average error of 14.09 % for the MA calculation. The averaging technique used to derive the mean host rock response has an error of 11.4 %. Thus the error imposed by the averaging is well within the limit of standard experimental error. The error analysis completely justifies this.

CONCLUSIONS

A comprehensive method to determine cleat spacings in coal was difficult to find. Existing methods for cleat aperture measurements in coal were inexact because the resolution was too low. Hence we developed a method based on a Gaussian Point Spread Function (PSF), to determine cleat aperture measurements from CT scans of coal samples. Peak height and missing attenuation measurements were used to generate the aperture distributions. In addition, a method to determine the cleat orientation and cleat spacing distribution from CT scans of coal samples was developed. Regarding the cleat orientation and relevant cleat spacings we observe configuration dependent spacing distributions in both samples, which can be used for fracture modeling in coal specimens up to one cubic foot in size. We are able to combine these two different techniques, for a better understanding of the cleat framework. Upscaling to seam size is not investigated. This combined procedure also proves that we are able to discriminate between the face cleat, the butt cleat and the bedding system.

However it should be remembered that, fractions of a pixel are not physical domains, and the length measurements within this domain can not be exact. Thus no measurement can be exact in the sub-pixel level, including the method described above. At best the error in the approximations can be reduced by chosing the right method.

NOMENCLATURE

I = transmitted intensity,

I_0 = incident intensity,

L = path length,

μ = measured linear attenuation coefficient,

μ_w = linear attenuation coefficient of water,

K = constant equal to 1000,

U = summed cleat length used for cleat spacing measument per spacing class,

F = frequency per spacing class,

G = grid spacing, distance between the line segments used for spacing measurement (4 pixels),

n = integer of the average accuracy range in pixels,

xp = position of the peak,

Δxp = width of the peak within a 68% confidence level,

CT_{coal} = mean CT response of the coal matrix,

ACKNOWLEDGEMENTS

This work was funded by the CO_2 sequestration RECOPOL project, the CATO-programme and NOW-NOVEM. Some of the samples used, were from the test site in Poland and France. My special thanks to Adri Maljaars, Henk van Asten and Leo Vogt for their technical support. We are also thankful to the technical support extended by the D. Bossie Codereanu of the Institute Francais du Petrol in Paris. The computer tomography would not have been possible without his help.

REFERENCES CITED

1. Ammosov, I.I., Eremin, I.V., 1963: Fracturing in Coal: IZDAT Publishers, Office of Technical Services, Washington, DC, 109 pp.

2. Bertheux, W.B., 2000: “Enhaced Coalbed Methane Production by Carbon Dioxide Injection in Water Saturated Coal”; Novem Technical Report, Contract no.222103/2008, 106 pp.

3. Close, J.C., Mavor, M.J., 1991: “Influence of coal composition and rank on fracture development in Fruitland coal gas reservoirs of San Juan Basin”; In: Schwochow, S., Murray, D.K., Fahy, M.F. (Eds.)., Coalbed Methane of Western North America, Rk. Mt. Assoc. Geol., Field Conf., 109--121.

4. Holman, J. P., 1994: Experimental Methods for Engineers: 6th Edition McGraw - Hill Inc.

5. Karacan, C.Ö., Okandan, E., 2000: “Fracture / cleat analysis of coals from Zonguldak Basin (northwestern Turkey) relative to the potential of coalbed methane production”; International Journal of Coal Geology 44, 109--125.

6. Keller, A. 1998: “High resolution, non-destructive measurement and characterization of fracture apertures”; International Journal of Rock Mechanics and Minning Sciences 35, 1037-1050.

7. Kendall, P.E., Briggs, H., 1933: “The formation of rock joints and the cleat of coal”; Proc. R. Soc. Edinburgh 53, 164--187.

8. Laubach, S.E., Marrett, R.A., Olson, J.E., Scott, R.A., 1998: “Characteristics and origins of cleat: a review”; International Journal of Coal Geology 35, 175--207.

9. Law, B.E., 1993: “The relation between coal rank and cleat spacing: implications for the prediction of permeability in coal”; Proc. Int. Coalbed Methane Symp., II, 435--442.

10. Stach, E., Mackowsky, M.Th., Teichmüller, M., Taylor, G.H., Chandra, D., Teichmüller, R., 1982: Stach's Textbook of Coal Petrology: Gebrüder Borntraeger, Berlin, 535 pp.

11. Taylor, J. R., 1997: An Introduction to Error Analysis: 2nd Edition University Science Books, Sausalito, California.

12. Ting, F.T.C., 1977: “Origin and spacing of cleats in coalbeds”; Journal of Pressure Vessel Technical Transactions ASME 99, 624--626.

13. Tremain, C.M., Laubach, S.E., Whitehead, N.H., 1991: “Coal fracture cleat.patterns in Upper Cretaceous Fruitland formation, San Juan Basin, Colorado and New Mexico: implications for exploration and development”; In: Schwochow, S., Murray, D.K., Fahy, M.F. (Eds.)., Coalbed Methane of Western North America. Rocky Mtn. Assoc. Geol, 49--59.

14. Vandersteen, K., Busselen, B., Van Den Abeele., Carmeliet, J. 2003: Quantitative characterization of fracture apertures using microfocus computed tomography. In: Mees, F., Swennen, R., Van Geet, M., Jacobs, P. (Eds.).: Applications of X-ray Computed Tomography in the Geosciences: Geol. Soc. Spec. Publ., 215, 61--68.

15. Van Geet, M. 2001: “Optimization of microfocus X-ray computer tomography for geological research with special emphasis on coal components (macerals) and fractures (cleats) characterization”; PhD thesis, K. U. Leuven, Belgium.

16. Verhelst, F., Vervoort, A., De Bosscher, PH., Marchal, G. 1995: “X-ray computerized tomography: determination of heterogeneities in rock samples”; Proceedings of the 8th International Congress on Rock Mechanics. Balkema, Rotterdam, 105-108.

17. Wolf, K. H. A. A., Ephraim, R., Siemons, N., Bosie-Codreanu, D. 2004 : “Analysing the cleat angle in coal seams using drilling cuttings and image analysis techniques”; Geologica Belgica 7, 3-4.

Samples	VRr (%)	Lipt. (%)	Vitrinite (%)	Inert. (%)	Moisture Cont (%)	Ash (%)	Min. Mat (%)	Vol. Matter (%)	Density (%)	TOC (%)
Brzeszcze 405	0.75	8.00	39.00	53.00	1.85	4.57	4.98	34.17	1.33	68.80
Silesia 155-315	0.68	7.00	70.00	24.00	7.00	20.05	21.85	40.13	1.38	60.73
Tupton	0.53	14.0	59.4	25.8		2.05	0.8	36.15		73.01

Table 1 Sample details

	Information on the entire stacks					Information on cleat orientations and relevant cleat lengths				
px = pixels	**nr. of images available**	**nr. of images measured**	**total nr. of cleats segm.**	**cleat length summed (px)**	**max. cleat length (px)**	**cleat orientation**	**total nr. of cleats segm.**	**sum oriented cleat lengths (px)**	**sum cleat lengths for spacings (px)**	**relevant cleat length (ratio)**
France 495										
XY	295	60	8926	130007	187	**0°** +/- 10°	3157	60132	33184	0.26
						90° +/- 10°	1859	27647	17592	0.14
ZX	130	26	1746	17513	112	**6°** +/- 15°	571	6251	1976	0.11
						94° +/- 10°	719	8611	3636	0.21
ZY	320	32	1531	27497	179	**0°** +/- 15°	330	4027	1200	0.04
						90° +/-15°	950	21764	14732	0.54
Brzeszce LW405										
XY	135	28	417	8412	108	**10°** +/- 10°	186	4248	644	0.08
						95° +/- 20°	102	2172	252	0.03
ZX	310	31	410	6625	120	**0°** +/- 20°	297	4982	620	0.09
						90° +/- 20°	79	1419	388	0.06
ZY	110	22	250	9666	205	**5°** +/- 20°	31	747	36	0.00
						92° +/- 20°	153	7980	3660	0.38

Table 2 Distribution of the total cleat length, relevant cleat length and orientation of the samples

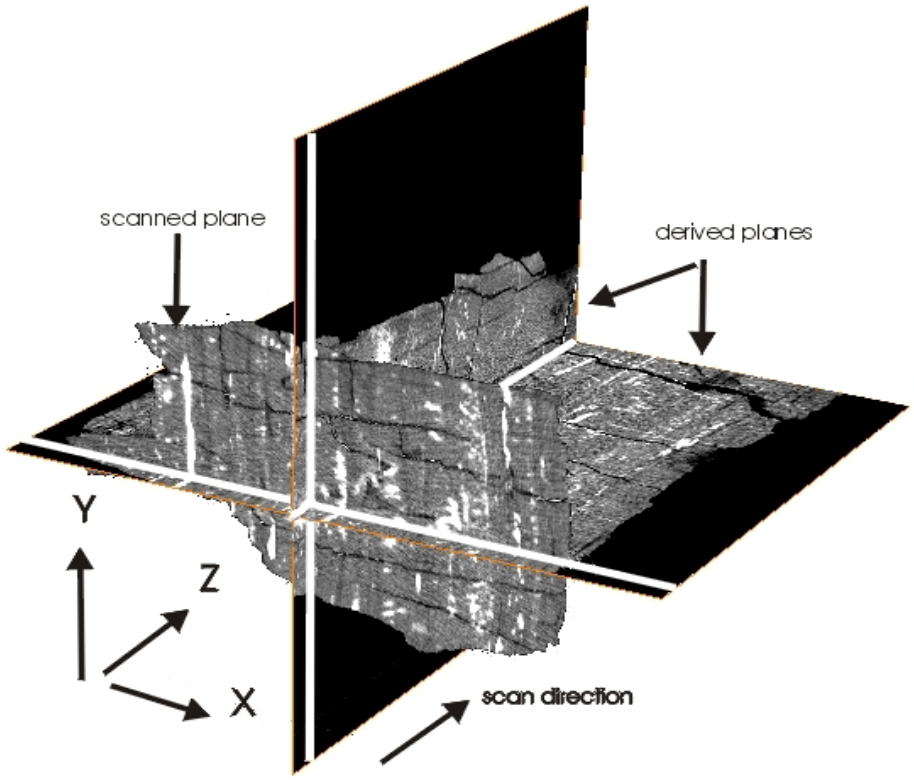

Figure 1 Orthoslices of France 495

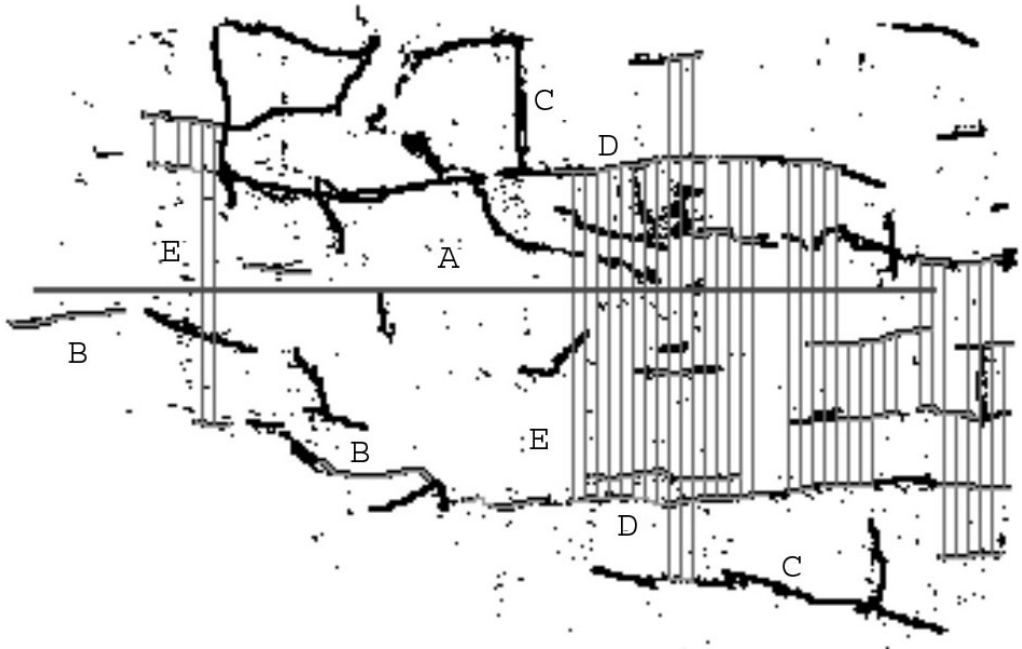

Figure 2 Cleat spacing measurements on a XY-section plane, showing all cleats after image analysis on cleat spacing. A. The chosen cleat direction, B. Cleats within the direction of choice without a parallel cleat for spacing measurements, C. For orientation neglected cleats, D. preferred cleats with parallel cleats for spacing measurements. E. Cleat spacing line segments

a)

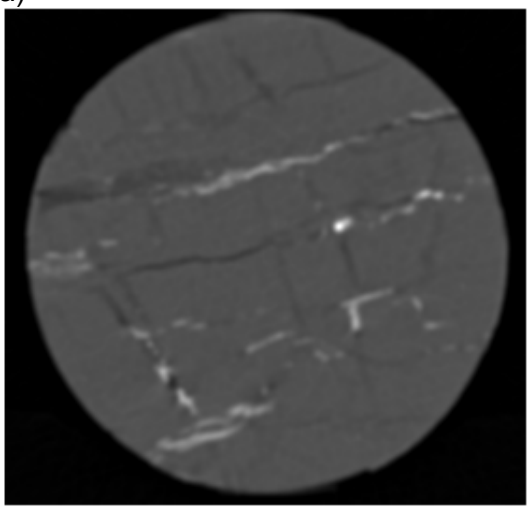

b)

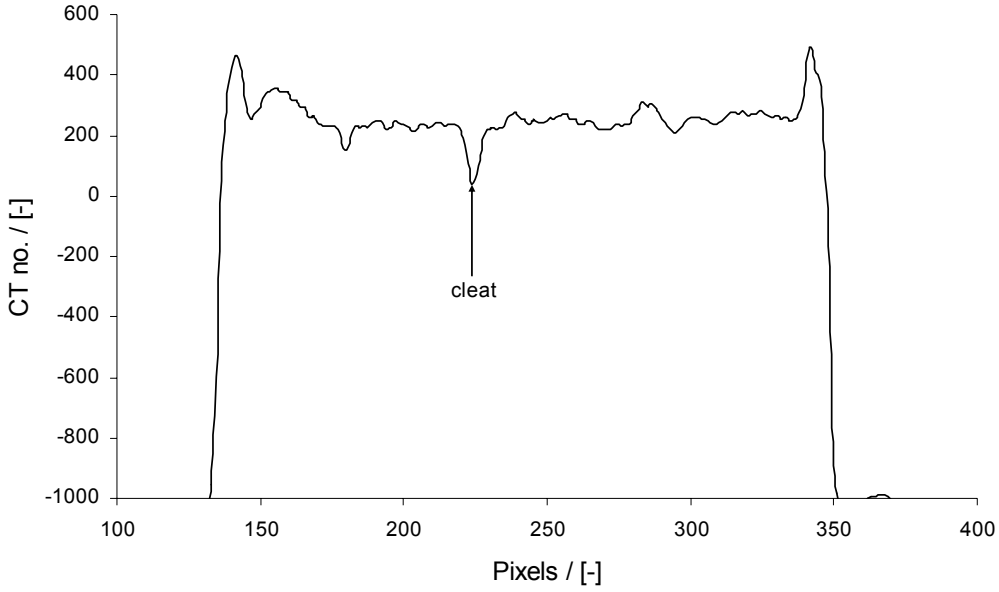

c)

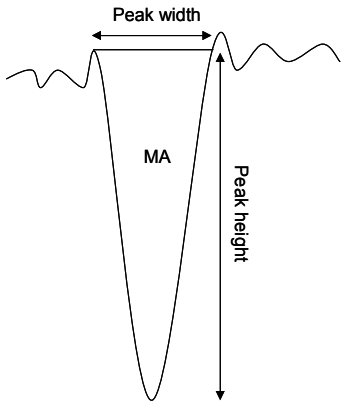

Figure 3 (a) CT image of a cleated coal core, (b) A profile across the CT image with a dip in the CT number showing the presence of a cleat and (c) Different methods to quantify a cleat aperture

a)

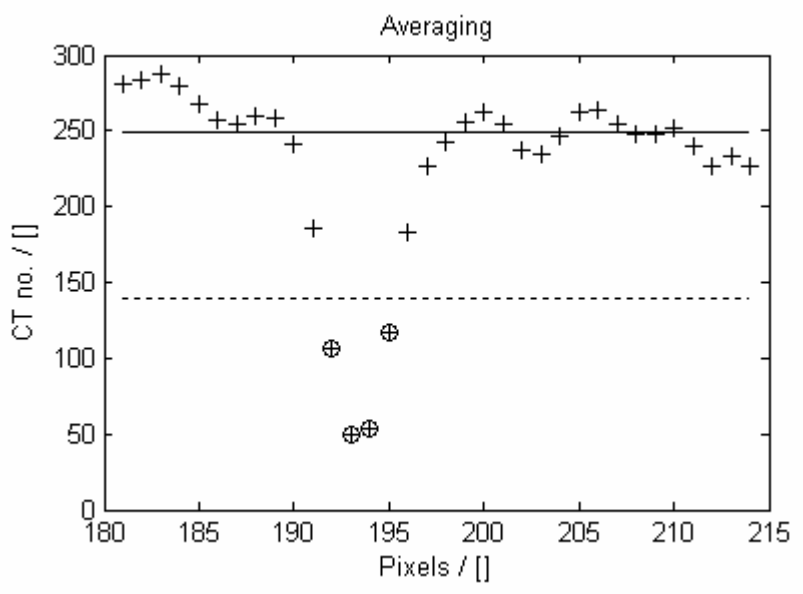

b)

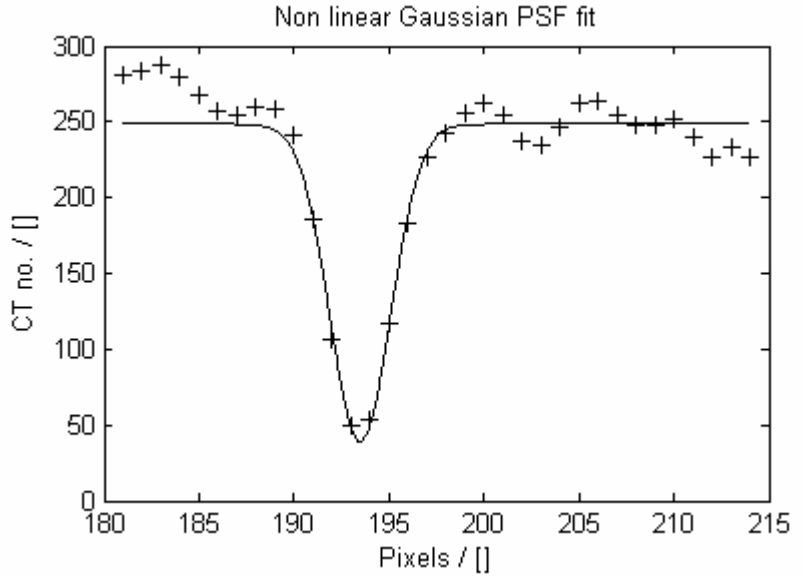

Figure 4 (a) The image of a cleat seen as the convolution of a rectangular fracture profile with a point spread function (PSF), which is Gaussian and (b) A fitting technique approximating the measured data

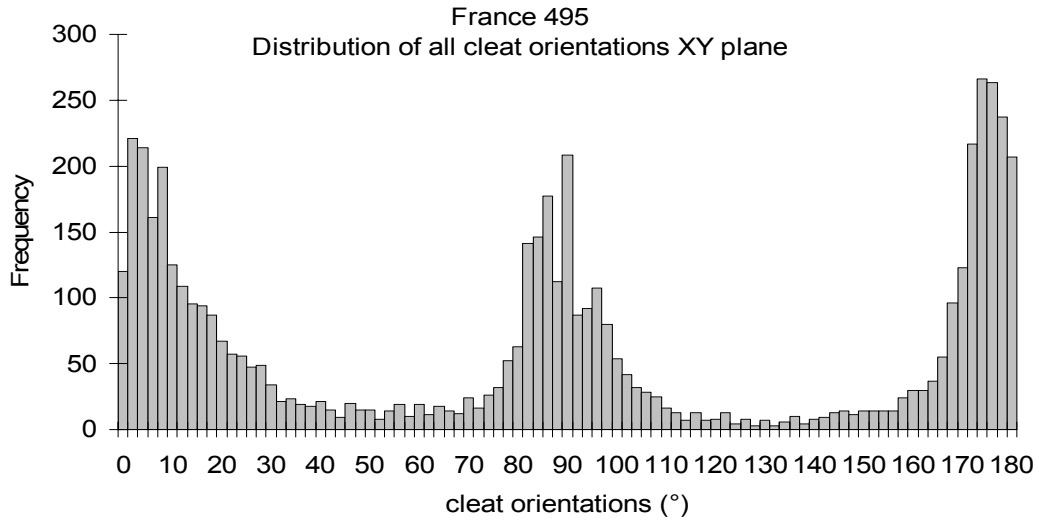

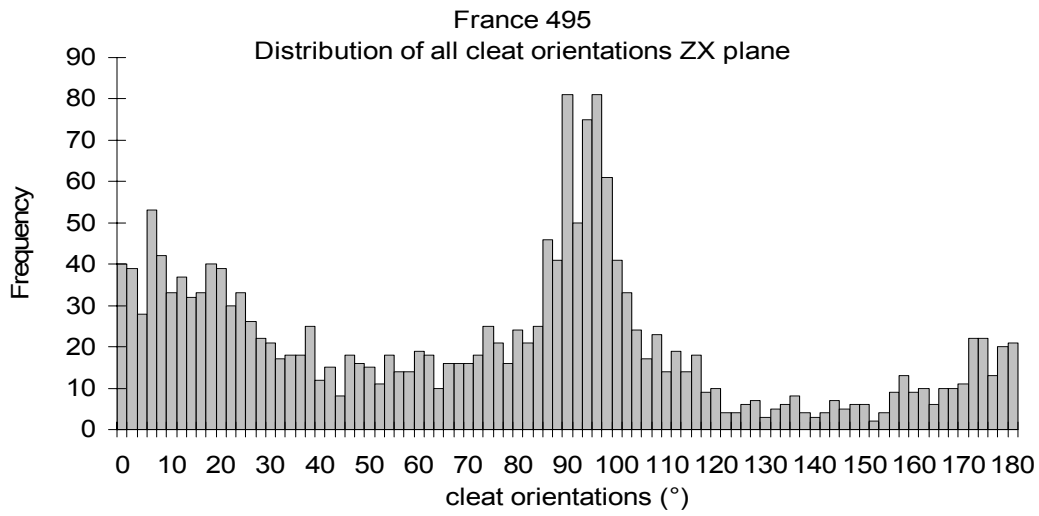

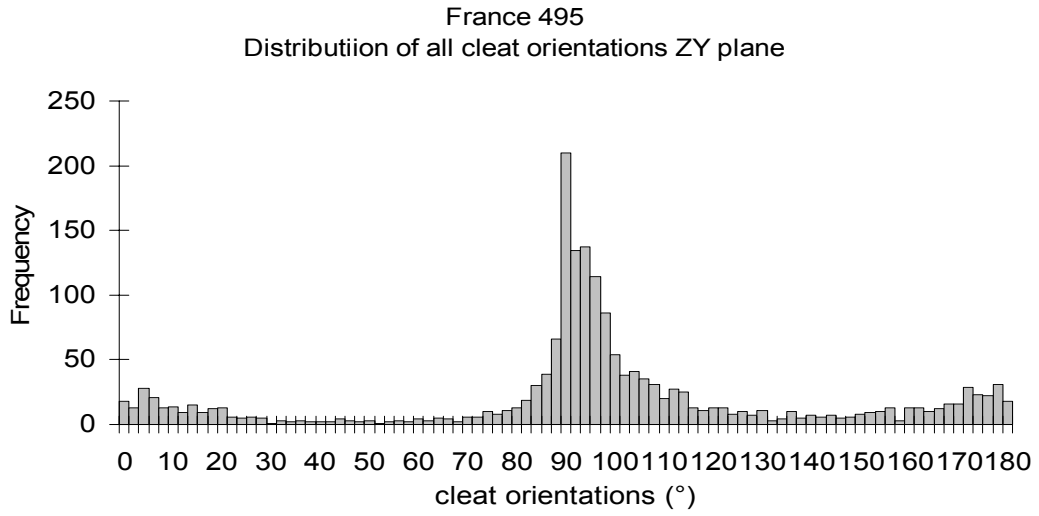

Figure 5 France 495. Distribution of all cleat orientations measured in the XY, ZX and ZY plane

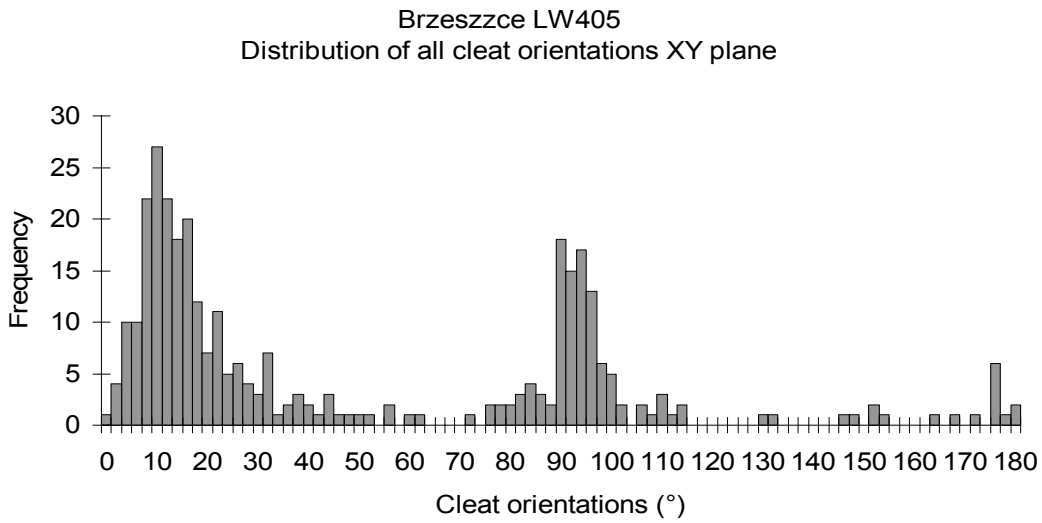

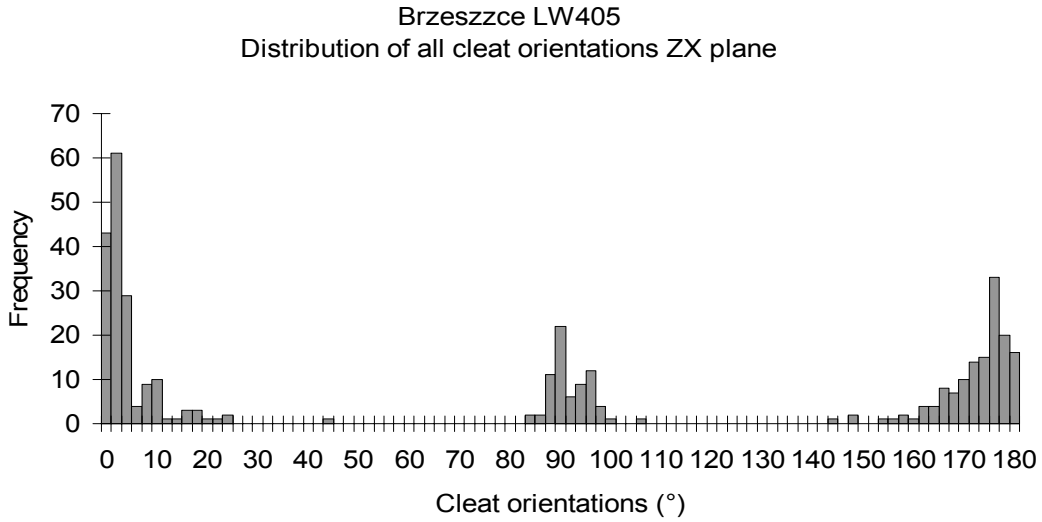

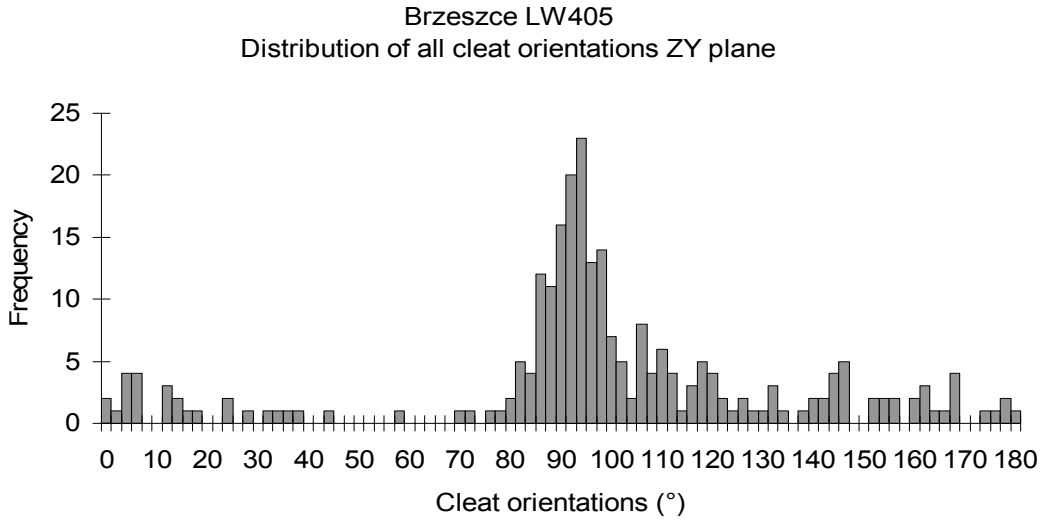

Figure 6 Brzeszce LW405. Distribution of all cleat orientations measured in the XY, ZX and ZY plane

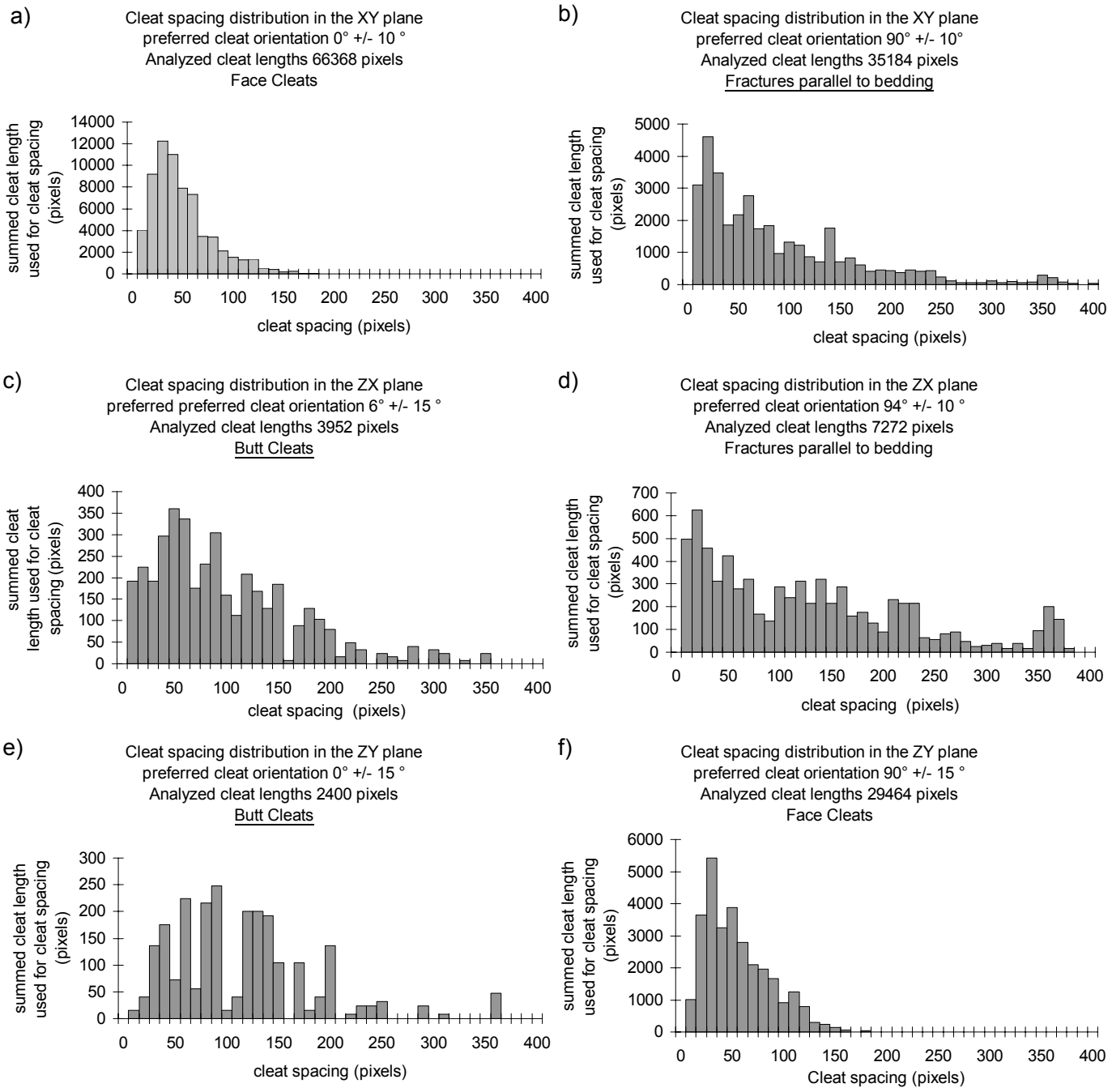

Figure 7 France 495. Distribution of cleat spacings against cleat lengths in the 3 orthogonal planes and in the two preferred cleat directions in each plane

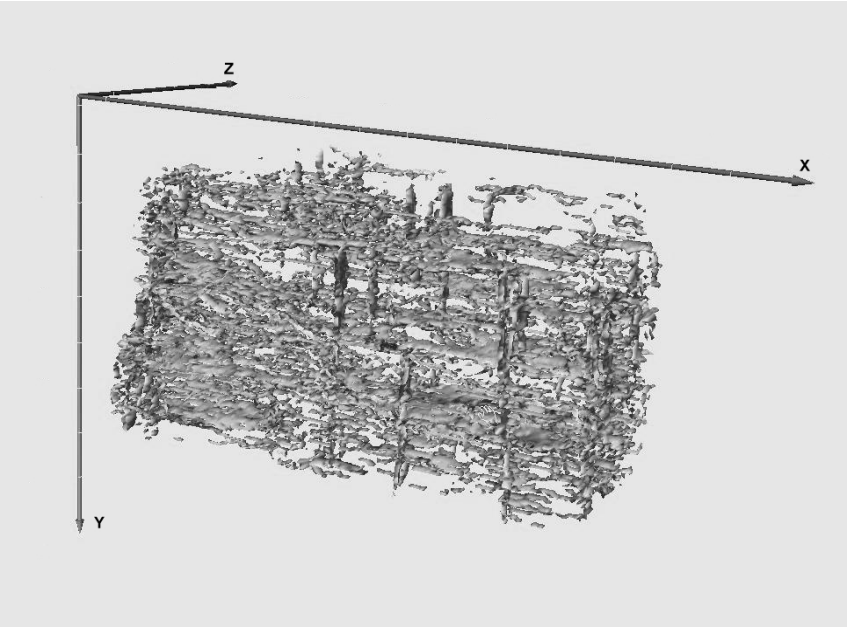

Figure 8 Rendered cleat system of France 495, using every 5th CT-scan in the stack direction (Z)

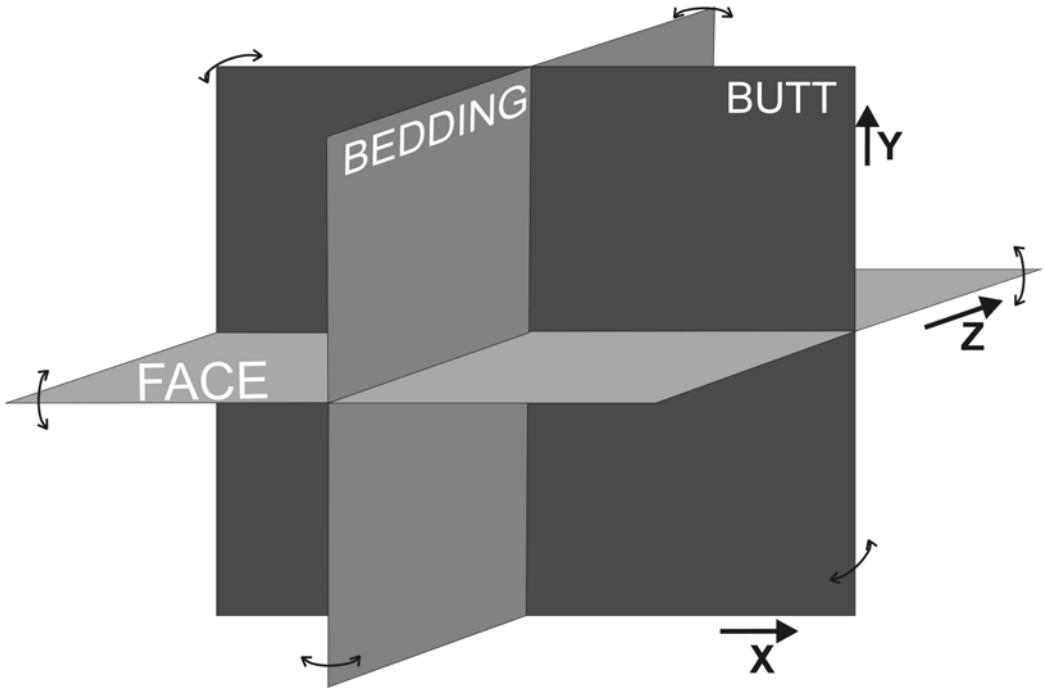

Figure 9 Orientation of the cleats and bedding related to the orientation of the CT-scan axis

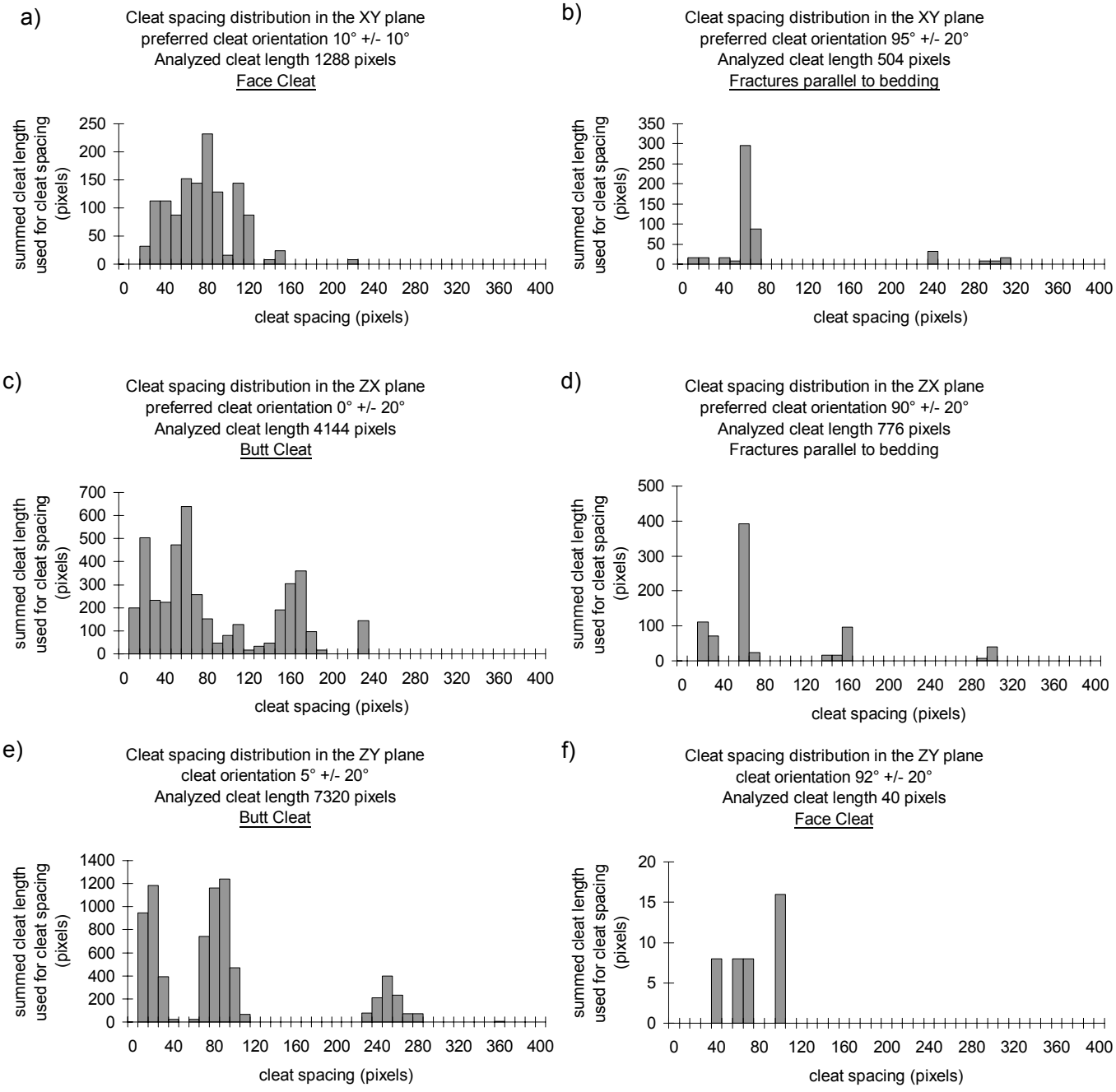

Figure 10 Brzeszce LW405. Distribution of cleat spacings against cleat lengths in the 3 orthogonal planes and in the two preferred cleat directions in each plane

a)

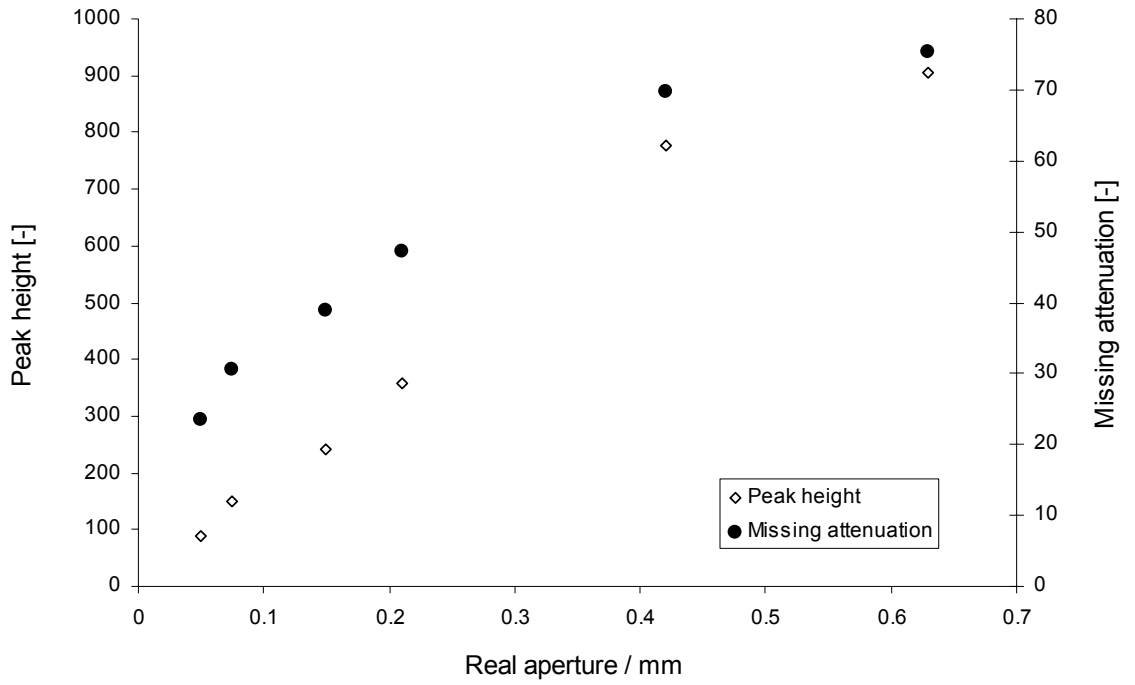

b)

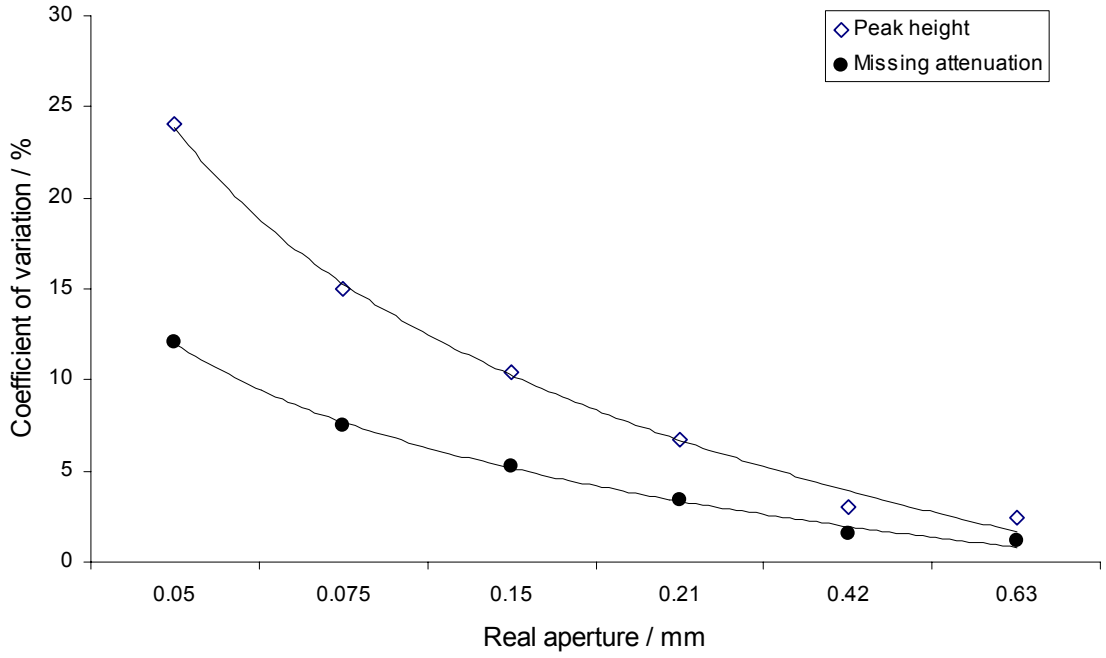

Figure 11(a) The calibration curves for peak height (*PH*) and missing attenuation (*MA*) and (b) A plot of the coefficient of variation for both peak height and missing attenuation as a function of the aperture width

a)

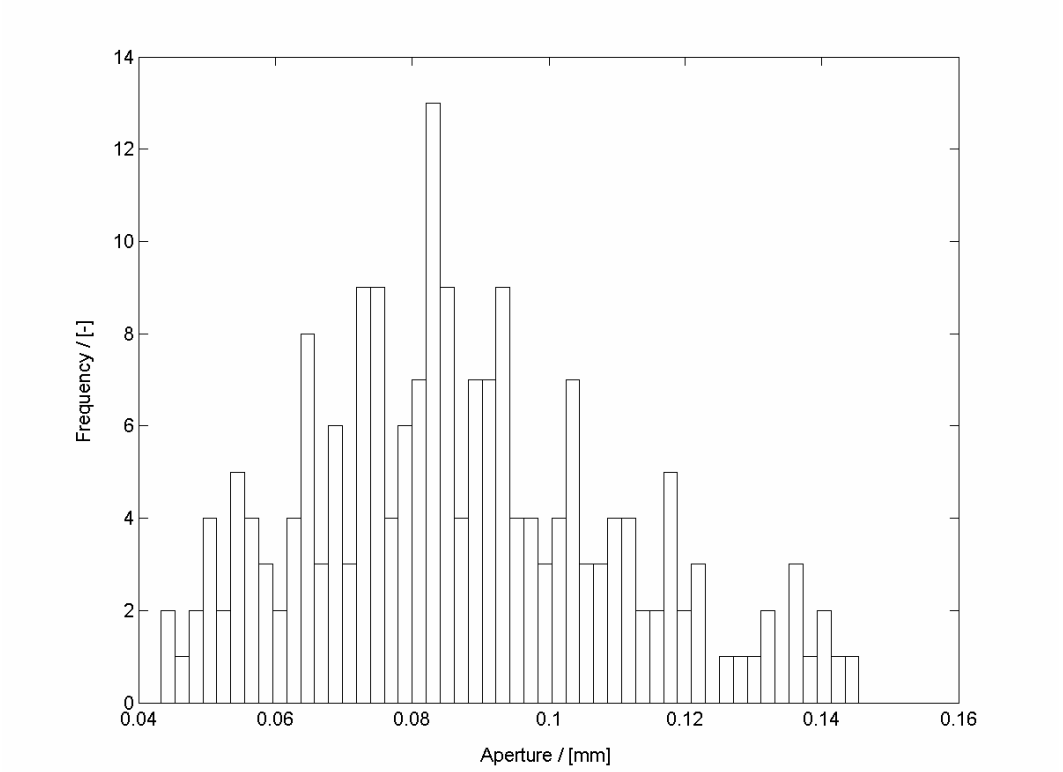

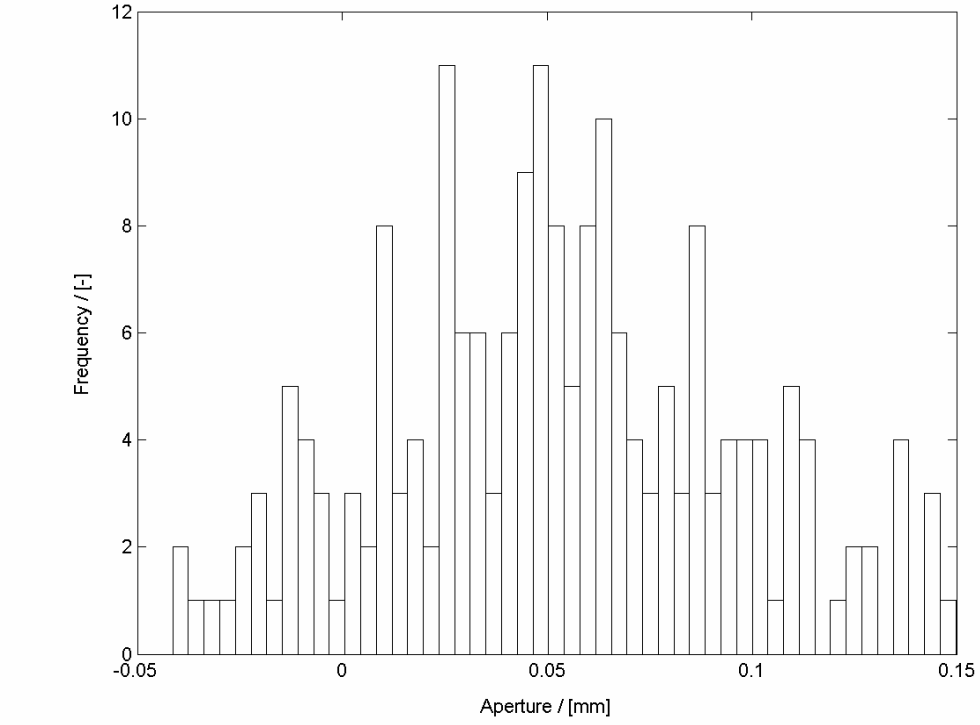

b)

Figure 12 Cleat aperture frequency distributions for the Silesia coal using (a) peak height and (b) missing attenuation as parameters to calculate the fracture aperture

a)

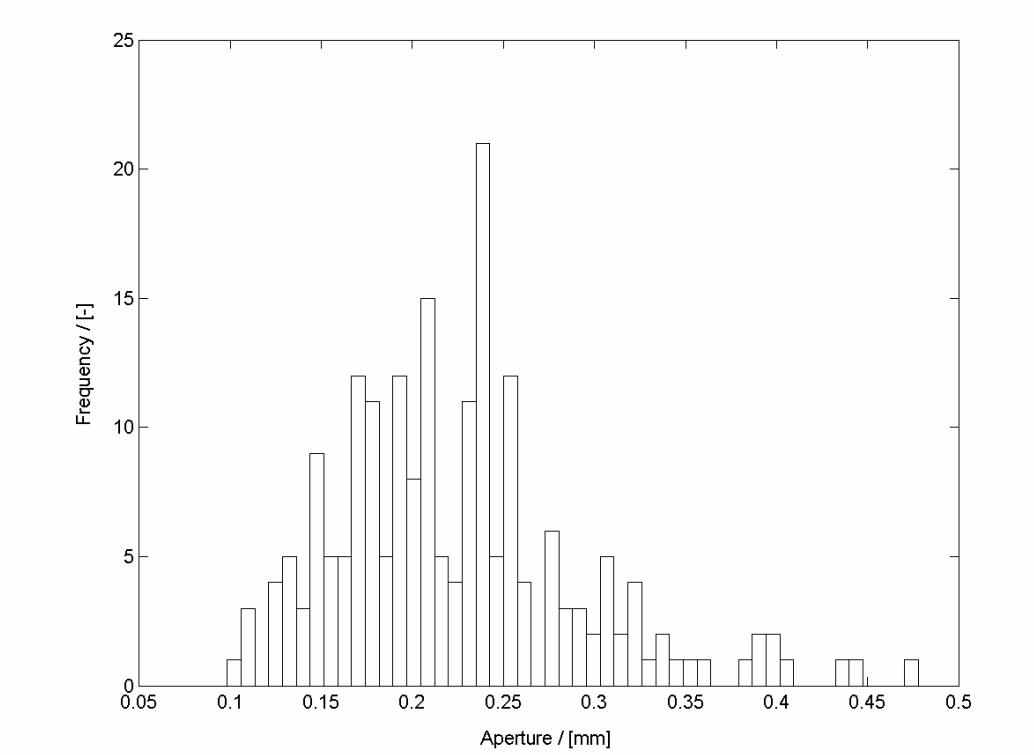

b)

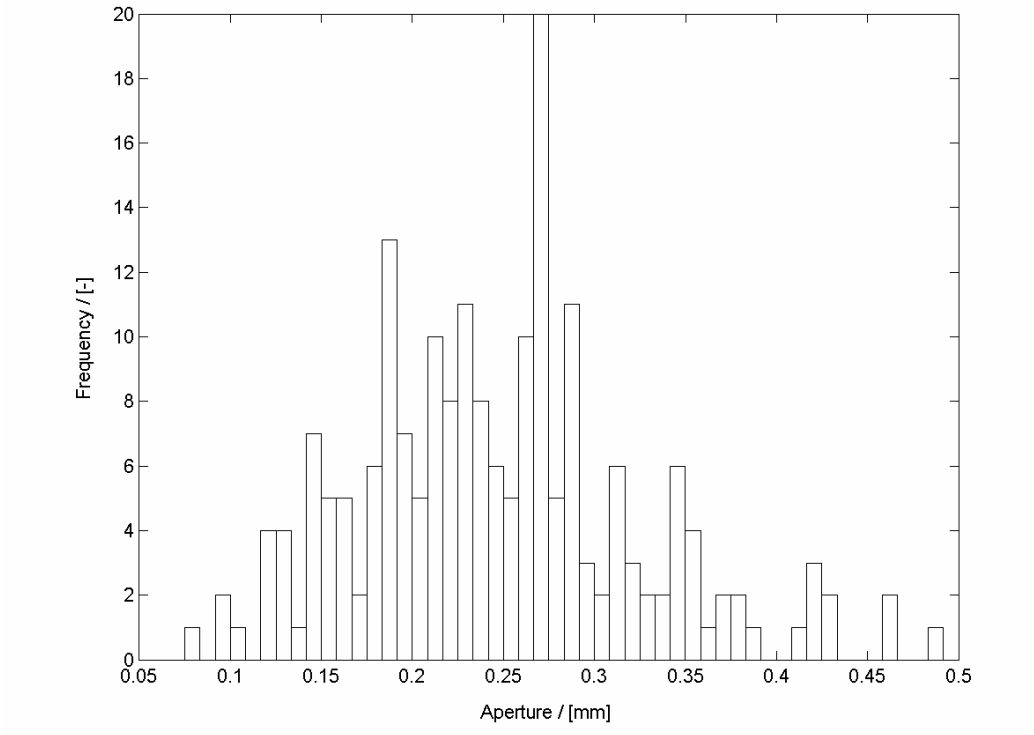

Figure 13 Cleat aperture frequency distributions for the Tupton coal using (a) peak height and (b) missing attenuation as parameters to calculate the fracture aperture

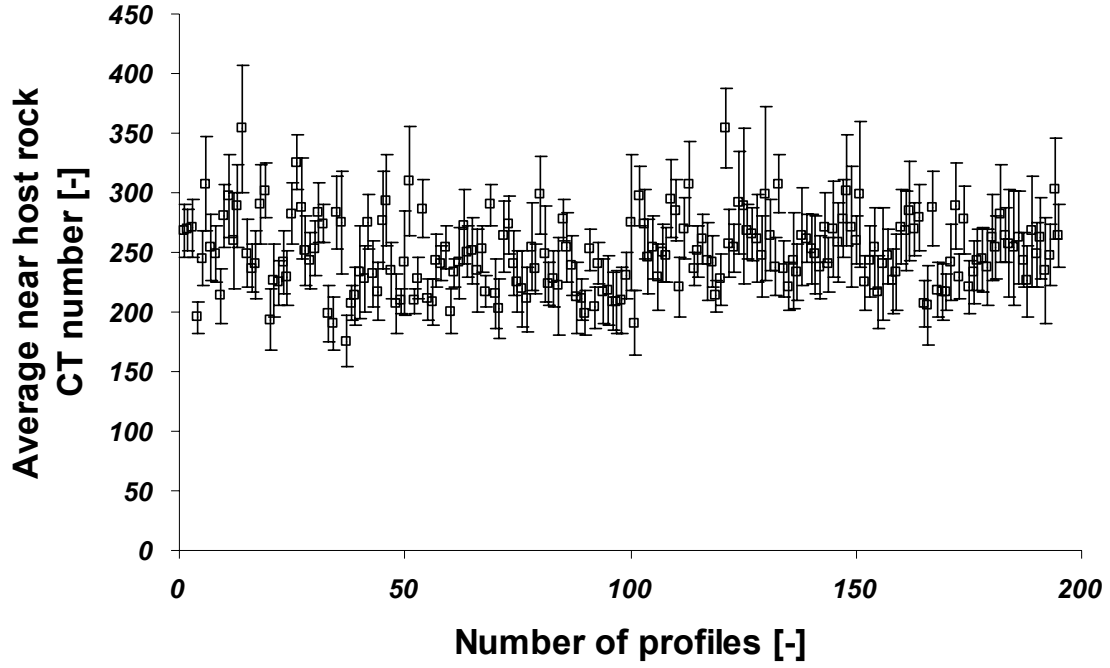

Figure 14 Error estimate of the average near host rock CT number for the Silesia coal sample

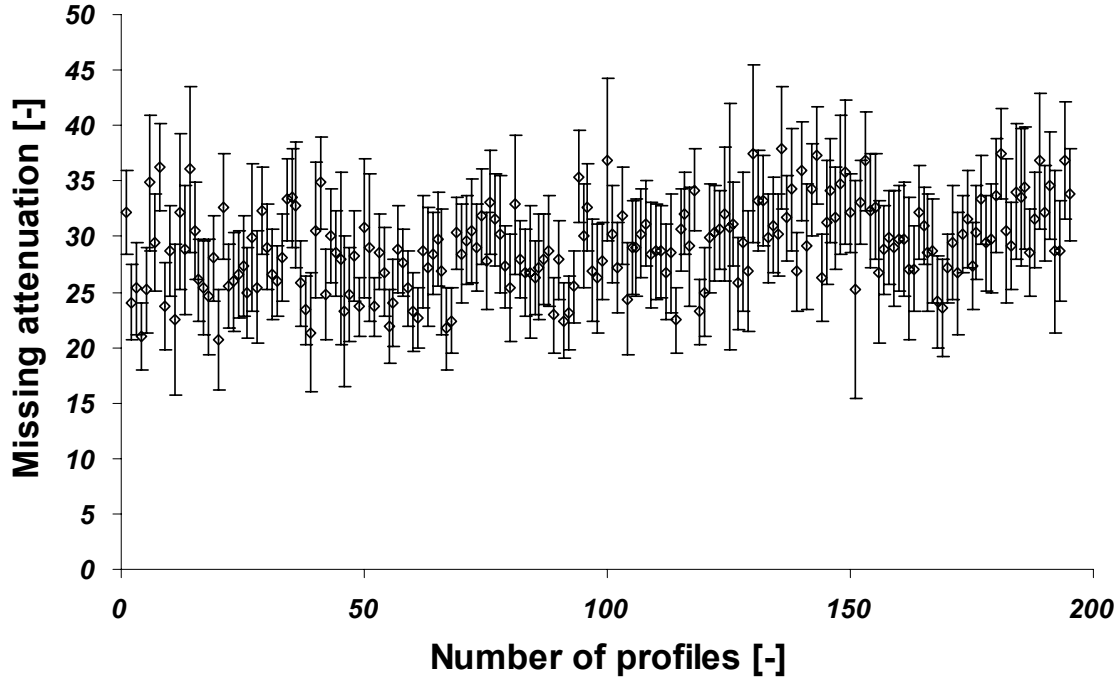

Figure 15 Error estimate of the missing attenuation (*MA*) for the Silesia coal sample